Full Paper Wiley Online Library ELECTROANALYSIS

DOI: 10.1002/elan.201600100

Non-enzymatic Amperometric Glucose Sensor Based on Copper Nanowires Decorated Reduced Graphene Oxide

Lele Ju,[a] Guosong Wu,[a] Biao Lu,[a] Xiaoyun Li,[a] Huaping Wu,[b] and Aiping Liu*[a, c]

Abstract: A nanocomposite consisting of one-dimensional copper nanowires and two-dimensional reduced graphene oxide nanosheets (CuNWs/rGO) was synthesized by a simple one-step wet-chemical synthetic process. The Cu NWs anchored onto the rGO nanosheets with wrinkles and folds had a smooth surface. The CuNWs/rGO hybrids exhibited excellent electrocatalytic activity toward glucose oxidation due to the superior conductivity along one-dimensional direction and excellent catalytic activity of Cu NWs and rapid electron transfer in the two-dimensional rGO sheets. A wide linear range up to 11 mM, high sensitivity (1625 μA/(mM·cm^2)), low detection limit (0.2 μM) and fast response (<2 s) to glucose oxidation were obtained under a working potential of 0.58 V for the hybrid with optimized Cu/rGO mass ratio in the alkaline solution. Furthermore, the CuNWs/rGO composites displayed high selectivity to glucose and resistance against poisoning by commonly interfering species such as ascorbic acid, dopamine, uric acid, acetamidophenol and some carbohydrates. The CuNWs/rGO hybrids with good reproducibility, stability and poisoning resistance to chloride ions were therefore promising for the potential application as non-enzymatic amperometric glucose sensors with improved electrochemical performances.

Keywords: Copper nanowire · Reduced graphene oxide · Hydrothermal synthesis · Non-enzymatic glucose sensor · Electrocatalytic activity

1 Introduction

Glucose, existing widely in blood of living beings, can be directly involved in the metabolic process in human body. The development of rapid, simple, sensitive and reliable methods for accurate glucose detection is important in many areas such as biotechnology, food industry, chemistry and environmental protection [1,2]. Due to the high sensitivity, simplicity and short response time, the electrochemical sensor is regarded as one of the most popular and effective methods for detecting glucose by the direct catalytic oxidation of glucose [3,4]. The first-generation glucose sensors based on enzymes have many drawbacks such as the intrinsic instability of enzymes, complexity and high cost [5–7]. By contrast, the low-cost, non-enzymatic glucose sensors are stable, highly sensitive with a low detection limit, and are therefore concerned greatly. Noble metal nanostructures such as gold, platinum, and palladium have been used as catalysts for constructing non-enzymatic glucose sensors. However, the expensive price of noble metals makes them difficult to a wide range of commercial application. Moreover, chloride ion, abundant existence in human blood, can poison the electrode materials, resulting in the loss of their activity [3]. In order to retain excellent catalytic activity and low-cost production, more attention has been focused on the Cu-based materials [7–31]. In recent years, various Cu-based nanostructures, such as monometallic and bimetal nanoparticles and nanorods [2,7–15,21–25], polyhedrons [26] and nanowires [28–31], have been synthesized for construction of non-enzymatic glucose sensors. These Cu-based materials not only show superior electrical conductivity but also resistant against a poison by chloride ion in the solution [7,21,24]. Particularly, the Cu nanowires (Cu NWs) as one-dimensional nanomaterials have been reported to be highly sensitive to glucose oxidation due to their excellent electron transfer along one-dimensional direction [32]. However, the single Cu NWs are instable and easy to oxidize with long-term use. Therefore, a catalyst support should be considered for use to improve the durability of catalysts [7,12,15,17–25,33].

The graphene (GE) or reduced graphene oxide (rGO) with high electrical conductivity, large specific surface area, distinguished mechanical properties and strong adhesion ability for metal catalyst is believed as an excellent catalyst support to improve activity and durability of catalysts [34]. Up to now, some studies based on the Cu/GE or Cu/rGO nanocomposite materials for glucose detection have been carried out. For example, Luo et al. adopted an electrochemically deposited method to synthesize Cu nanoparticles on the GE sheets modified glassy carbon electrode for glucose detection [27]. Fan et al. fab-

[a] L. Ju, G. Wu, B. Lu, X. Li, A. Liu
Center for Optoelectronics Materials and Devices, Zhejiang Sci-Tech University, Hangzhou 310018, China
*e-mail: liuaiping1979@gmail.com

[b] H. Wu
Key Laboratory of E&M (Zhejiang University of Technology), Ministry of Education & Zhejiang Province, Hangzhou 310014, China

[c] A. Liu
State Key Laboratory of Nonlinear Mechanics, Institute of Mechanics, Chinese Academy of Sciences, Beijing 100190, China

ricated Cu NWs modified GE transparent electrode through spin-coating Cu NWs onto GE surface and confirmed the excellent catalytic activity for glucose oxidation [31]. However, most researches related to CuNW-based catalysts for glucose sensing usually adopt a two-step synthesis procedure, namely CuNWs preparation and CuNW-catalyst support recombination, which is complicated and time-consuming. Additionally, the protection role of GE or rGO to the Cu NWs from oxidation is not well investigated.

In this work, we fabricate CuNWs/rGO hybrids through a facile, one-step wet-chemical synthetic approach. The effect of rGO content on the structures, catalytic performance and long-term stability of CuNWs/rGO hybrids is carefully investigated by changing the quality ratio of GO to Cu-based precursor. The CuNWs/rGO hybrid displays fascinating sensitivity, fast amperometric response, excellent selectivity and wide detection range for glucose oxidation due to the superior conductivity along one-dimensional direction and excellent catalytic activity of Cu NWs and rapid electron transfer in the two-dimensional rGO sheets. The synergistic effect of Cu NWs and rGO favors the hybrids significant electrocatalytic activity toward glucose oxidation when compared to the single rGO or Cu NWs. The good reproducibility and long-term stability of the hybrids are contributed to the protection role of rGO to the Cu NWs.

2 Experimental

2.1 Materials

Sodium hydroxide (NaOH), copper nitrate ($Cu(NO_3)_2 \cdot 3\,H_2O$), ethylenediamine (EDA), hydrazine (N_2H_4 35 wt%), potassium ferricyanide ($K_3[Fe(CN)_6]$), potassium chloride (KCl), dopamine (DA), ascorbic acid (AA), uric acid (UA), acetamidophenol (AP), fructose, sucrose and Nafion were purchased from Sigma-Aldrich. Other reagents were commercially available and of analytical reagent grade. Graphite powder (256 mesh) was supplied by Qingdao Huatai Tech. Co. Ltd. Deionized water with resistance of approximately 18 MΩ·cm was used throughout the experiment.

2.2 Preparation of Cu NWs and CuNWs/rGO Hybrids

The GO was prepared from natural graphite powder by using modified Hummers' method [35]. Cu NWs were synthesized by using the modified method reported in the previous work [36]. Typically, 20 mL of concentraed NaOH solution (15 M) in a flask was pre-heated to 60 °C, followed by dropwise addition of 1 mL $Cu(NO_3)_2$ solution (0.1 M). The resulting solution was stirred for 15 min and then 0.16 mL EDA and 25 μL N_2H_4 solution (35 wt%) were injected into the flask. The flask was capped and maintained at 60 °C for 1.5 h, followed by cooling down to room temperature in an ice bath. The reddish production was filtered and washed with excessive ice water. Finally, the as-prepared Cu NWs were dried in a vacuum oven.

In a typical process of CuNWs/rGO synthesis, a 9 mg GO powder was dispersed in 3 mL deionized water. Then the suspension (3 mg/mL) was sonicated for 1h in order to disperse the GO uniformly. A $Cu(NO_3)_2$ solution (1 mL, 0.1 M) in a glass vial was mixed with different amounts of GO, namely 0.107 mL, 0.213 mL and 0.427 mL (corresponding to the quality ratio of GO to Cu of 0.05, 0.1 and 0.2), respectively, and the obtained three vials were labeled as S_1, S_2 and S_3, respectively. After adding 0.16 mL EDA, the color of solutions changed from blue to dark violet with sequentially sonicated for 10 min again. Then the dark violet solutions were dropwise added into pre-heated NaOH (20 mL, 15 M) at 60 °Cwith stirring. After that, 35 μL, 45 μL and 65 μL N_2H_4 solution (35 wt.%) were injected into the S_1, S_2 and S_3 flasks, respectively, and the three flasks were capped and maintained at 60 °C for 1.5 h without stirring, followed by cooling down to room temperature. The productions were washed and collected by centrifugation in deionized water and ethanol in order to remove the excess alkali and unreacted reagents, respectively.

For electrode preparation, the ITO-coated glasses were sonicated in ethanol and deionized water for 10 min, respectively, and dried in N_2. 3 mg CuNWs/rGO hybrid was mixed with 1mL ethanol and 20 μL Nafion solution (5 wt% in ethanol), and then the dispersion was ultrasonically treated to form the ink (catalyst dispersion). After that, 20 μL ink was dropped onto the ITO electrode with the average apparent area 0.4 cm^2 (0.8 cm × 0.5 cm) and subsequently dried under vacuum for 2 h at room temperature. The Cu NWs or rGO modified electrodes as comparison were also prepared in a similar way.

2.3 Characterization and Measurements

The morphologies of different hybrids were observed by a Field emission scanning electron microscope (FESEM, Hitachi S4800). The X-ray diffraction (XRD) pattern was obtained on a diffractometer (Bruker AXS D8) using the Cu Ka radiation (λ = 0.15418 nm) with the 2θ scan from 10° to 80° at a step of 0.02°. The Raman spectra of GO and CuNWs/rGO on silica wafers were collected by a Thermo Fisher DXR Raman spectrometer with a He-Ne laser (λ = 632.8 nm). The Fourier transform infrared (FTIR) spectra of GO and CuNWs/rGO were recorded using a Bruker Tensor 27 spectrometer with samples embedded in KBr disks. The XPS core level spectra and elemental composition of different samples were collected by the X-ray photoelectron spectroscopy (XPS, KRATOS AXIS ULTRA-DLD) with the binding energies calibrated by C1s as reference energy (C1s = 284.6 eV). The electrochemical measurements were carried out with a CHI660B electrochemical workstation (Shanghai Chenhua Instrument Factory, China) in a three-electrode cell, which consisted of a working electrode, a platinum wire as the counter electrode, and Ag/AgCl (3 M KCl) elec-

trode as the reference electrode, respectively. The behavior of glucose oxidation on the working electrode was investigated by cyclic voltammetry (CV) at a potential range from 0.1 V to 0.8 V, chronoamperometry (I-T) and electrochemical impedance spectroscopy (EIS) technique. The supporting electrolyte in CV and I-T experiments was 0.1 M NaOH solution with nitrogen saturated. All currents obtained on the electrodes were normalized to the apparent area of each electrode with same catalyst loading.

Table 1. Element contents of different catalysts obtained from XPS measurement.

Catalyst	Element content (wt.%)		
	C	O	Cu
rGO	64.6	35.4	–
Cu NWs	–	3.8	96.2
CuNWs/rGO (S_1)	30.7	16.7	52.6
CuNWs/rGO (S_2)	34.8	19.2	46.0
CuNWs/rGO (S_3)	41.5	23.1	35.4

3 Results and Discussion

3.1 Microstructures of Cu NWs and CuNWs/rGO Hybrids

During the preparation process of Cu NWs and CuNWs/rGO hybrids, the EDA is necessary as the structure-directing agent to promote the anisotropic growth of Cu NWs from copper spherical seeds which were reduced from copper complexes of $Cu(OH)_4^{2-}$ by N_2H_4 in the high concentrated alkaline solution [36]. Fig. 1 displays typical SEM images of GO nanosheet, Cu NWs and CuNWs/rGO composites. The GO nanosheets have some wrinkles and folds on the surfaces and edges (Fig. 1a). The Cu NWs are uniform with an average diameter of 100 nm and the length from dozen to dozens of micrometer (Figs. 1b). As shown in the high-magnification SEM image (Fig. 1c), the surface of 100-nm-diameter Cu NWs is smooth. For the CuNWs/rGO hybrids, the Cu NWs are anchored onto the rGO nanosheets. With the increase of GO amount, the Cu NWs on the rGO sheet become loose and the connection degree among these Cu NWs is weakened (Figs. 1d–f). Table 1 displays the element contents of different catalysts. The content ratio of carbon element to the oxygen one (C : O) is about 1.8 ± 0.1 for the three CuNWs/rGO catalysts, which is similar to the value

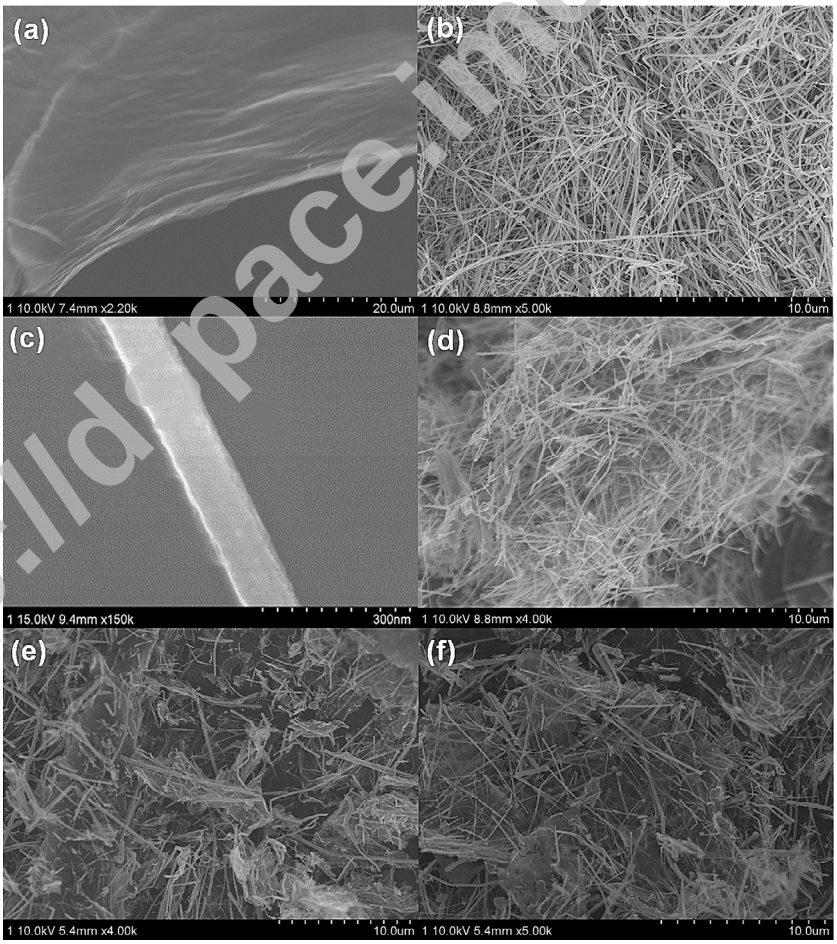

Fig. 1. Scanning electron microscopy images of (a) GO sheets, (b)–(c) Cu NWs, and (d)–(f) CuNWs/rGO composites based on S_1, S_2 and S_3, respectively.

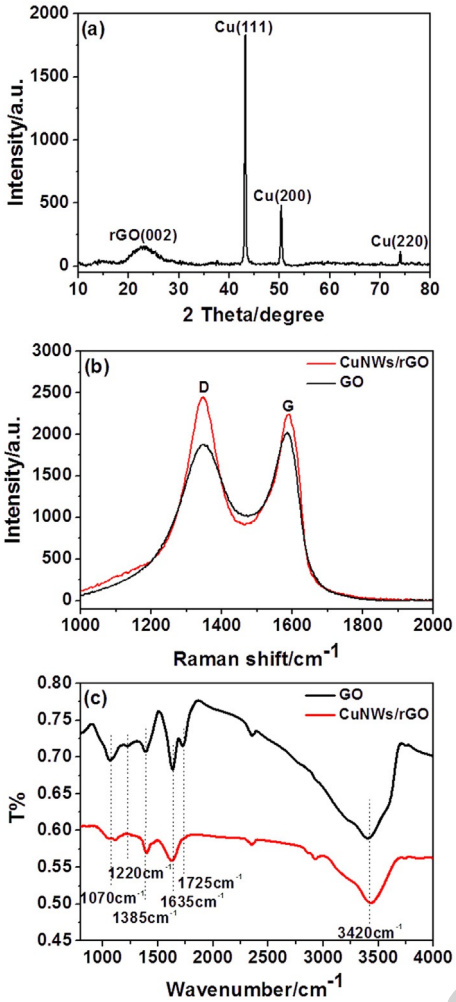

Fig. 2. (a) XRD pattern of CuNWs/rGO (S_2) composites, (b) Raman spectra and (c) FTIR spectra of GO and CuNWs/rGO (S_2) composites.

of pure rGO. This hints that the incorporation of Cu NWs in the rGO does not introduce extra oxygen component. Therefore, the Cu NWs obtained in our synthesis is neat and the oxygen signal observed in the Cu NWs catalyst might be attributed to the oxygen absorbed on the Cu NWs.

Fig. 2(a) shows the XRD pattern of CuNWs/rGO (S_2) composites. The broad characteristic peak at 23.1° indicates the successful reduction of GO to rGO with poor ordering along its stacking direction [37]. The diffraction peaks located at 43.3°, 50.4° and 74.1° perfectly match the (1 1 1), (2 0 0) and (3 1 1) crystalline planes of Cu with face-centered cubic crystal structure (JCPDS 04-0836), respectively. The absence of the diffraction peaks of CuO and Cu_2O implies the pure Cu NWs in production. From the Raman spectra of GO and CuNWs/rGO (S_2) composites shown in Fig. 2(b), the GO and rGO display two prominent peaks at 1345 cm^{-1} and 1588 cm^{-1}, corresponding to the D-bands (arising from the tangential stretch of sp^2-hybridized carbon) and the G-bands (representing the crystalline graphite with E_{2g} zone center mode), respectively [38]. The intensity ratios of D-band to G-band (I_D/I_G) increase from 0.93 for GO to 1.10 for CuNWs/rGO, suggesting more defects introduced into rGO. From the FTIR of GO in Fig. 2(c), three characteristic peaks at 1070 cm^{-1} (ν_{C-O}), 1635 cm^{-1} ($\nu_{C=C}$) and 1725 cm^{-1} ($\nu_{C=O}$) reveal the existence of oxygen-containing functional groups in the GO. However, the peaks ($\nu_{C=O}$ and ν_{C-O}) disappear or are weakened in the FTIR of CuNWs/rGO (S_2), implying the amount of oxygen-containing functional groups is remarkably less after GO reduction by hydrazine.

EIS is a useful tool to study characteristic of electrode related to electron transfers between the electrolyte and the electrode surface. It is proposed that the semicircle diameter at higher frequencies reflects the electron-transfer resistance [39]. Fig. 3 shows the EIS results in Nyquist plots for bare ITO, ITO-Nafion, ITO-Nafion-rGO, ITO-Nafion-CuNWs and ITO-Nafion-CuNWs/rGO (S_2) electrodes, and the corresponding equivalent circuit model. The R_S is defined as the series resistance of the system and represents the ohmic resistance of electrolyte between the electrode and Luggin capillary and that within the pores of the catalysts. The R_{CT} is the charge transfer resistance between the solid-liquid interface. Our simulated results show that the values of R_{CT} for different electrodes increase in the order of bare ITO (4 Ω) < ITO-Nafion-CuNWs/rGO (6 Ω) < ITO-Nafion-CuNWs (13 Ω) < ITO-Nafion-rGO (24 Ω) < ITO-Nafion (34 Ω). After modifying ITO electrode with Nafion, the R_{CT}

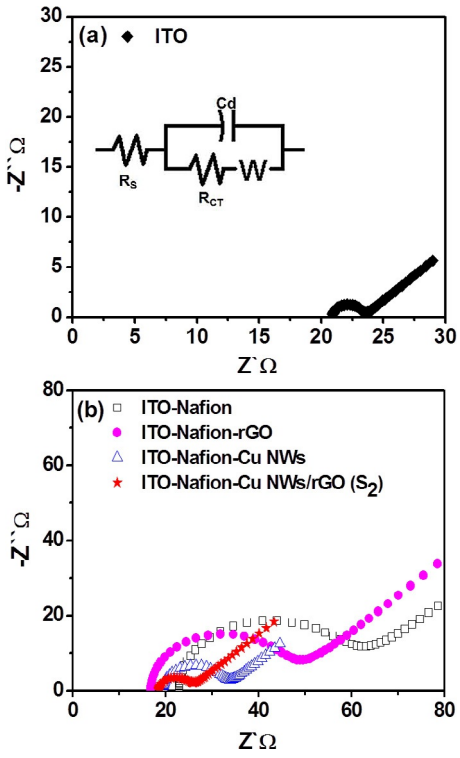

Fig. 3. Electrochemical impedance spectra of (a) ITO glass and (b) different electrodes in the 0.1 M KCl electrolyte solution containing 0.01 M $Fe(CN)_6^{3-/4-}$.

value increases remarkably owing to the Nafion hindering in the interfacial charge transfer. The ITO-Nafion-rGO and ITO-Nafion-CuNWs electrodes have lower resistances when compared to the ITO-Nafion electrodes due to the good conductivity of rGO and Cu NWs. The CuNWs/rGO (S_2) composites exhibit smaller semicircle diameter at high frequencies and lower electron-transfer resistance due to the synergistic effect of one-dimensional Cu NWs and two-dimensional rGO sheets.

3.2 Electrochemical Activities of CuNWs/rGO Hybrids

The electrocatalytic activities of rGO, Cu NWs and CuNWs/rGO composites are investigated in 0.1 M N_2-saturated NaOH solution with and without 2 mM glucose at a scan rate of 50 mV/s. No current related to glucose oxidation can be found on rGO modified electrode (Fig. 4a). For the Cu NWs modified electrode, the background current increases with the potential scanning towards positive direction. When 2 mM glucose is added to the reaction system, an apparent shoulder peak at about 0.55 V with a rapid increase in current is observed, which corresponds to the oxidation of glucose (Fig. 4a). The possible oxidation mechanism of glucose at Cu-modified electrode in the alkaline media is proposed by the following steps [31,40]:

$$Cu + 2OH^- \rightarrow CuO + H_2O + 2e^-, \quad (1)$$

$$CuO + OH^- \rightarrow CuOOH + e^- \quad (2)$$
$$\text{or } CuO + H_2O + 2OH^- \rightarrow Cu(OH)_4^- + e^-,$$

$$Cu(III) + \text{glucose} + e^- \rightarrow \text{gluconolactone} + Cu(II), \quad (3)$$

$$\text{gluconolactone} + Cu(II) \rightarrow \text{gluconic acid (hydrolysis)} + Cu(II). \quad (4)$$

The Cu(0) is electrochemically oxidated to Cu(II) species through the transition of Cu(0)/Cu(II) at the negative potential [41] and further oxidated to Cu(III) species such as CuOOH or $Cu(OH)_{4<brtr-}$ at about 0.55 V, which are considered as the strong oxidizing agent for glucose oxidation. Moreover, the Cu(III) species are consumed in the electrooxidation of glucose as confirmed by the absence of peak related to the transition of Cu(III)/Cu(II) in the cathodic scan (Fig. 4a). Therefore, rGO has no contribution to direct nonenzymatic glucose detection while Cu NWs play a primary role in the electroxidation process of glucose. For CuNWs/rGO hybrids with different amounts of rGO, a rapid increase in current starting at 0.3 V with an obvious oxidation peak generated at around 0.58 V is collected due to the glucose oxidation (Fig. 4b) when the 2 mM glucose is added into the system. In contrast to the Cu NWs, the CuNWs/rGO hybrids exhibit higher current response relative to own background current, indicating a stronger electrocatalytic

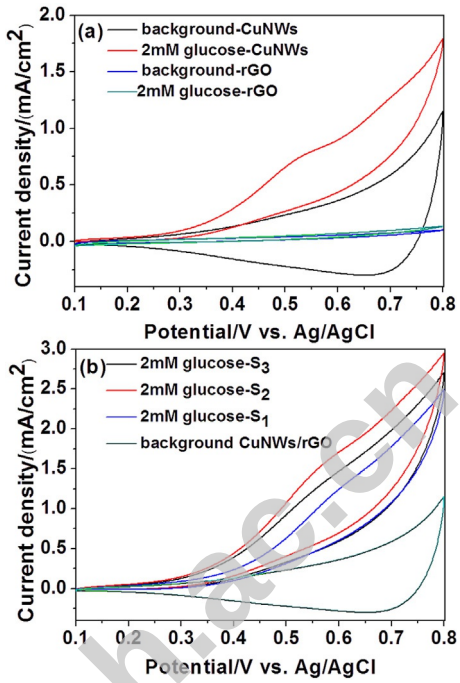

Fig. 4. (a) Cyclic voltammograms of Cu NWs and rGO modified electrodes in 0.1 M N_2-saturated NaOH with and without 2 mM glucose, respectively. (b) Cyclic voltammograms of CuNWs/rGO composites (S_1, S_2 and S_3) modified electrodes in 0.1 M N_2-saturated NaOH with and without 2 mM glucose, respectively.

capacity toward the oxidation of glucose. The remarkable electrocatalytic activity of CuNWs/rGO hybrids may originate from the superior conductivity along one-dimensional direction and excellent catalytic activity of Cu NWs and rapid electron transfer in the two-dimensional rGO sheets. It is worth noting that the current response of CuNWs/rGO hybrids modified electrodes based on S_1 and S_3 are lower than that based on S_2. This means that a suitable amount of GO not only guarantees the tight junctions between Cu NWs but also exposes sufficient Cu active sites for glucose oxidation.

The electrochemically effective surface area of CuNWs/rGO modified electrode has been calculated according to the method provided by Liu et al. [42]. First, the effective surface areas of the bare ITO and rGO/ITO electrodes are estimated to be 0.234 and 0.490 cm^2, respectively, by using $K_3[Fe(CN)_6]$ as a model complex (Fig. 5) according to the general Randles-Sevcik equation [43]. Since the CuNWs in the CuNWs/rGO composite would react with $K_3[Fe(CN)_6]$, the effective surface area of CuNWs/rGO electrode can be calculated according to the relation of electrical double layer capacitance with effective surface area based on cyclic voltammetry measurements (Fig. 6) [44]. Our calculated results reveal that the CuNWs/rGO modified electrodes based on S_1, S_2 and S_3 have larger effective surface areas (1.518, 1.719 and 1.617 cm^2, respectively) than ITO and rGO/ITO ones, which further contribute to their good electrochemical activities for glucose detection.

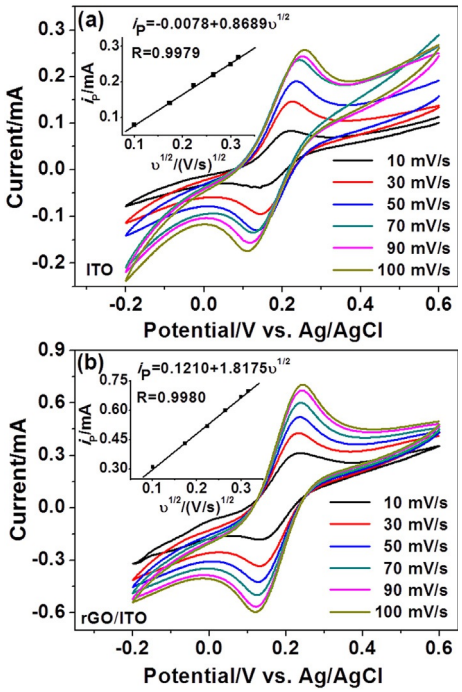

Fig. 5. Cyclic voltammograms of (a) ITO and (b) rGO/ITO electrodes in 0.1 M KCl containing 5 mM $K_3[Fe(CN)_6]$ at different scan rates (v). Insets are the relations of anodic i_P versus $v^{1/2}$.

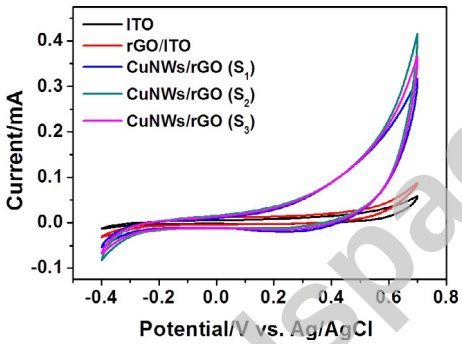

Fig. 6. Cyclic voltammograms for different electrodes in 0.1 M NaOH at a scan rate of 0.1 V/s.

It is generally known that the working potential affects the amperometric response of sensors. Therefore, we explore the effect of working potential on the electrochemical behaviors of CuNWs/rGO (S_2) composites modified electrodes with successive addition of 0.1 mM glucose in the 0.1 M N_2-saturated NaOH solution at 50 s interval. As shown in Fig. 7, the maximum step-like current response is observed at 0.58 V. For the working potential higher or lower than 0.58 V, the oxidative current response is lower. Moreover, a higher potential may favor the oxidation of intermediate interferents. Hence, the optimal working potential is 0.58 V for CuNWs/rGO catalysts.

Fig. 8 shows the current-time (I-T) curves of CuNWs/rGO composites modified electrodes based on S_1, S_2 and

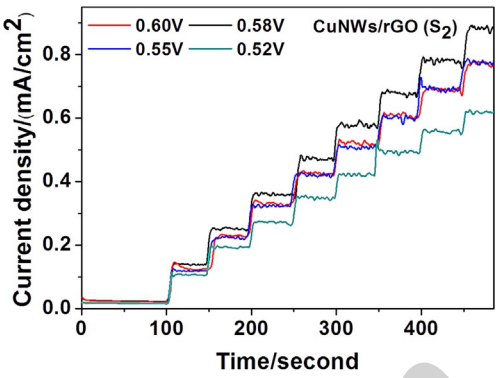

Fig. 7. Amperometric responses of CuNWs/rGO (S_2) composites modified electrodes at different potentials with successive addition of 0.1 mM glucose in the 0.1 M N_2-saturated NaOH solution at 50 s interval.

S_3 samples by successive injection of glucose solution into the 0.1 M N_2-saturated NaOH solution at 0.58 V, and the corresponding calibration plots are displayed in Fig. 8(c) and Fig. 8(f), respectively. As successive injection of glucose, the CuNWs/rGO composites modified electrodes present large step-like increase of current density, which reaches the steady-state equilibrium within 2 s, indicating an attractive short response time. This might result from the superior conductivity along one-dimensional direction of Cu NWs and rapid electron transfer in the two-dimensional rGO sheets. Moreover, compared to the I-T curves of $S_1$and S_3, the current density of glucose oxidation obtained from S_2 is higher obviously and the detection range for glucose concentration is wider. The corresponding sensitivity, correlation coefficient, linear response range, and detection limit (S/N = 3) are summarized in Table 2. One can see that the CuNWs/rGO composites modified electrode based on S_2 has the highest sensitivity (1625 μA/(mM·cm^2)), the lowest detection limit (0.2 μM) and the widest detection range (1 μM–11 mM) to glucose oxidation since a small amount of GO can not guarantee the close interlinking between Cu NWs and rGO, while a large amount of GO may impede the transport of glucose molecules to the active sites on the Cu NWs. A performance comparison of the CuNWs/rGO composites modified electrodes based on S_2 with those of reported non-enzymatic glucose sensors is shown in Table 3. It is clear that our sensor based on the CuNWs/rGO hybrids exhibits exciting characteristics of high sensitivity, low detection limit and wide response range and therefore is

Table 2. Sensor properties of different CuNWs/rGO composites modified electrodes.

Catalyst	Linear response range	Sensitivity (μA/(mM·cm^2))	Detection limit (μM)	R^2
S_1	5 μM–9 mM	600	1.6	0.988
S_2	1 μM–11 mM	1625	0.2	0.993
S_3	5 μM–9 mM	1075	0.6	0.990

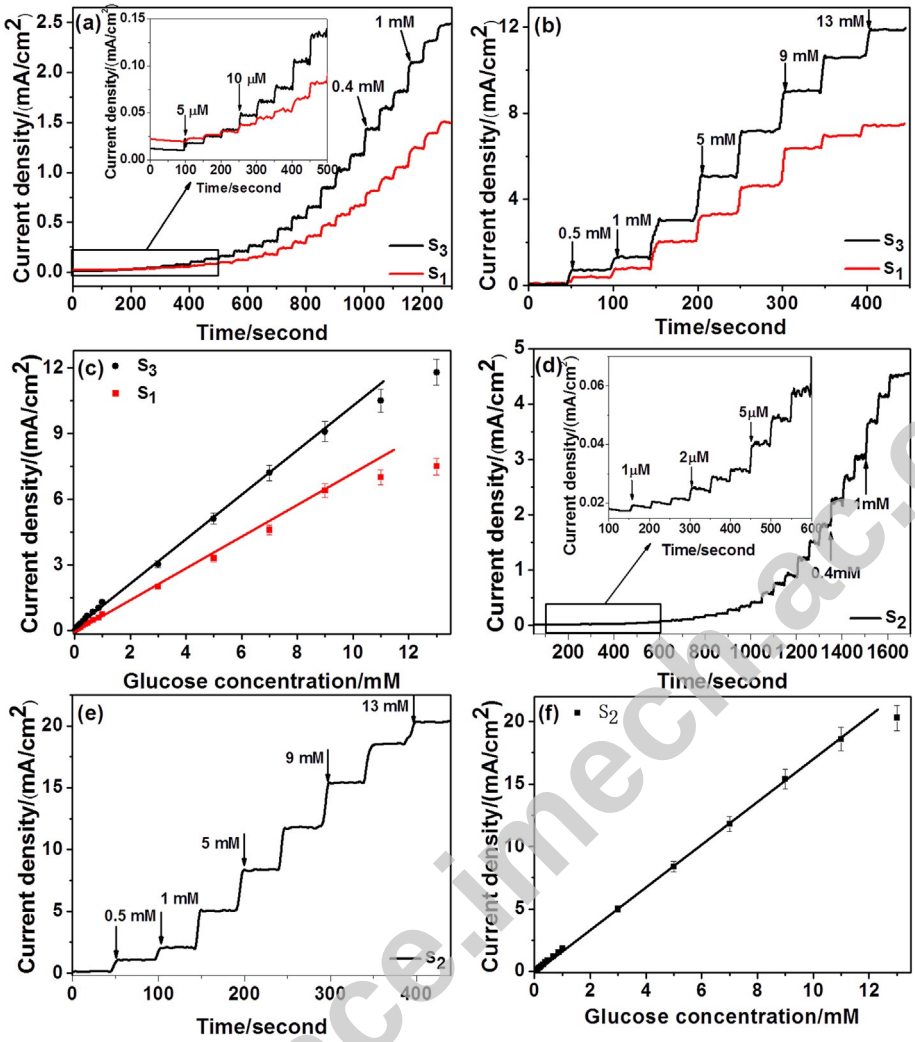

Fig. 8. (a)–(b) Amperometric responses of CuNWs/rGO composites modified electrodes based on S_1 and S_3 for successive addition of various-concentration glucose in the 0.1 M N_2-saturated NaOH solution at 0.58 V. (c) Corresponding calibration curves of (a) and (b). (d)–(e) Amperometric response of CuNWs/rGO composites modified electrode based on S_2 for successive addition of various-concentration glucose in the 0.1 M N_2-saturated NaOH solution at 0.58 V. (f) Corresponding calibration curve of (d) and (e). The insets in (a) and (d) are amplified I-T curves. Error bars in (c) and (f) indicate the relative standard deviations of six measurements. The line indicates the calibration curve.

promising for the determination of blood sugar concentration in the practical clinical analysis.

3.3 Reproducibility, Stability and Anti-interference Property of CuNWs/rGO Based Sensor

The reproducibility of the developed sensor is evaluated by measuring the current response of five CuNWs/rGO composite modified electrodes upon 0.1 mM glucose in 0.1 M N_2-saturated NaOH solution with a relative standard deviation (RSD) of 4.3%. Meanwhile ten successive addition of 0.1 mM glucose is measured for the same electrode with the RSD of 2.1%. These results indicate that the CuNWs/rGO composite based sensor has a good reproducibility. The stability and antioxidant capacity of the developed sensor is investigated by measuring the current response to glucose oxidation (1 mM) and element contents after three months. It can be seen that the current response obtained from CuNWs/rGO (S_2) decreases by 8% and 17% after ten days and three months, respectively, when compared to the initial current. While the current response obtained from Cu NWs decreases by 15% and 36% at the same time interval when compared to the initial current (Fig. 9). The RSD up to 4.0% is calculated based on six measurements at the different catalysts modified electrode. Furthermore, the mass ratio of Cu/O displays a significant decrease with time lengthening for the Cu NWs catalyst after exposed to ambient condition when compared to that of the CuNWs/rGO (S_2). This implies that the rGO layer could effectively protect the Cu NWs from oxidation during a long-term employment.

Additionally, many interfering species such as AA, DA, UA, AP and some carbohydrates (fructose and sucrose)

Table 3. Performance comparison of various non-enzymatic glucose sensors.

Electrode	Working potential (V)	Linear response range	Sensitivity	Detection limit (μM)	Reference
Cu NWs/rGO	0.58	1 μM–11 mM	1625 μA $mM^{-1}cm^{-2}$	0.2	this work
Cu NWs/GTE	0.6	5 μM–6 mM	1100 μA $mM^{-1}cm^{-2}$	1.6	[31]
Cu NWs/MWCNTS	0.55	1 μM–3 mM	1995 μA $mM^{-1}cm^{-2}$	0.26	[30]
Cu NWs	0.6	0.1 μM–3 mM	420.3 μA $mM^{-1}cm^{-2}$	0.035	[28]
Cu NPs/graphene	0.5	4 μM–4.5 mM	48.13 μA mM^{-1}	1.3	[24]
Cu nanocubes/MWCNTS	0.55	3 μM–7.5 mM	1096 μA $mM^{-1}cm^{-2}$	1	[45]
Cu@C NWs	0.65	0.05 M–3 mM	437.8 μA $mM^{-1}cm^{-2}$	0.05	[46]
Cu nanoclusters	0.65	1 μM–5 mM	17.76 μA mM^{-1}	0.5	[47]
CuO NPs/GO	0.7	2.79 μM–2.03 mM	262.5 μA $mM^{-1}cm^{-2}$	0.69	[39]
Cu_2O nanocunes/graphene	0.6	0.3 mM–3.3 mM	285 μA $mM^{-1}cm^{-2}$	3.3	[48]

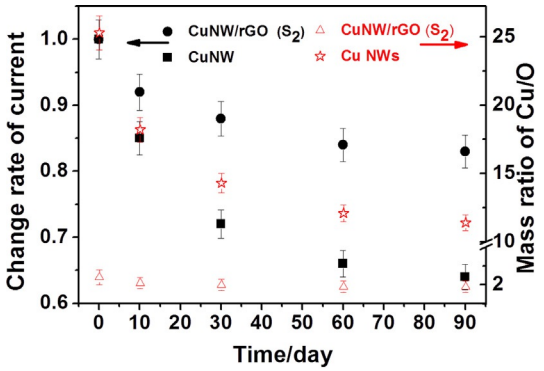

Fig. 9. Dependences of change rate of current related to glucose oxidation (1 mM) and mass ratio of Cu/O of different catalysts on exposure time. Error bars indicate the relative standard deviations calculated based on six measurements at the Cu NWs and CuNWs/rGO (S2) catalysts modified electrode.

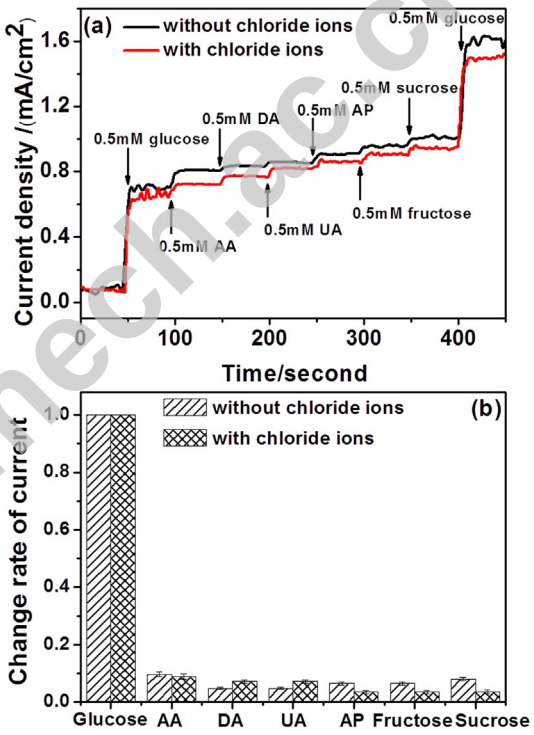

Fig. 10. (a) Interference test of CuNWs/GO (S_2) composite modified electrodes in the 0.1 M N_2-saturated NaOH solution with and without chloride ions at 0.58 V with the addition of 0.5 mM glucose, 0.5 mM ascorbic acid (AA), 0.5 mM dopamine (DA), 0.5 mM uric acid (UA), 0.5 mM acetamidophenol (AP), 0.5 mM fructose and 0.5 mM sucrose. (b) Current rate of current of interferences related to glucose oxidation. Error bars indicate the relative standard deviations calculated based on six measurements.

coexist with glucose in real physiological samples. Therefore, the anti-interference property is an important factor for biosensors. The interference experiment of CuNWs/rGO (S_2) composite based sensor is executed by the addition of 0.5 mM glucose and 0.5 mM AA, UA, DA, AP, fructose and sucrose, respectively, as shown in Fig. 10. The current response produced by the oxidation of interfering species does not show any significant effect to the glucose oxidation after the second addition of glucose, suggesting the high specificity to glucose detection using CuNWs/rGO hybrids. When the 0.1 M KCl solution is added in the NaOH solution, only 5–8% reduce in current can be detected, indicating the good poisoning resistance of the catalyst to the environment containing chloride ions, as reported by previous studies [7,24].

The analysis capability of the developed sensor for the real sample is investigated by adding 20.0 μL of human serum sample obtained from a local hospital in the 5.0 mL of 0.1 M N_2-saturated NaOH solution. The current response for glucose at 0.58 V is determined by the RSD of pure glucose to the solutions containing the serum samples, and the RSD recorded by the injections of 0.5 mM glucose in five solutions is calculated to be about 4.1%. Our results show that this glucose biosensor based on CuNWs/rGO hybrids is suitable for the determination of real serum samples.

4 Conclusions

A series of CuNWs/rGO composites were fabricated by a one-step wet chemical approach for the exploitation of non-enzymatic glucose sensors. The content of rGO in CuNWs/rGO composites had great impact on the performance of non-enzymatic glucose sensors. The CuNWs/rGO composite electrode with optimized Cu/rGO mass ratio displayed wide linear range (1 μM–11 mM), high sensitivity (1625 μA/(mM·cm^2), low detection limit (0.2 μM), fast response (<2 s), satisfactory reproducibility

and good selectivity for glucose oxidation in the alkaline solution even containing chloride ions. The simple and low-cost synthesis procedure of CuNWs/rGO hybrid and its excellent properties make it potential application for non-enzymatic amperometric glucose sensors.

Acknowledgements

This work was supported by the National Natural Science Foundation of China (Grant Nos. 51272237, 51572242 and 11372280), the Zhejiang Provincial Natural Science Foundation of China (Grant No. LY16E020011), the 521 Talent Project of Zhejiang Sci-Tech University and the Program for Innovative Research Team of Zhejiang Sci-Tech University, the Opening Fund of State Key Laboratory of Nonlinear Mechanics and the Program for Innovative Research Team of Zhejiang Sci-Tech University (Grant No. 15010039-Y).

References

[1] N. Mitro, P. A. Mak, L. Vargas, C. Godio, E. Hampton, V. Molteni, A. Kreusch, E. Saez, *Nature* **2007**, *445*, 219–223.
[2] Q. Chen, L. Zhang, G. Chen, *Anal. Chem.* **2011**, *84*, 171–178.
[3] J. Wang, *Chem. Rev.* **2008**, *108*, 814–825.
[4] X.-C. Dong, H. Xu, X.-W. Wang, Y.-X. Huang, M. B. Chan-Park, H. Zhang, L.-H. Wang, W. Huang, P. Chen, *ACS nano* **2012**, *6*, 3206–3213.
[5] P. Si, Y. Huang, T. Wang, J. Ma, *RSC Adv.* **2013**, *3*, 3487–3502.
[6] X.-M. Chen, Z.-J. Lin, D.-J. Chen, T.-T. Jia, Z.-M. Cai, X.-R. Wang, X. Chen, G.-N. Chen, M. Oyama, *Biosens. Bioelectron.* **2010**, *25*, 1803–1808.
[7] M. Yuan, A. Liu, M. Zhao, W. Dong, T. Zhao, J. Wang, W. Tang, *Sens. Actuators B* **2014**, *190*, 707–714.
[8] L. Chen, T. Fujita, Y. Ding, M. Chen, *Adv. Funct. Mater.* **2010**, *20*, 2279–2285.
[9] H. Li, C.-Y. Guo, C.-L. Xu, *Biosens. Bioelectron.* **2015**, *63*, 339–346.
[10] S. Xu, H. Li, L. Wang, Q. Yue, S. Sixiu, J. Liu, *CrystEngComm* **2014**, *16*, 9075–9082.
[11] M.-M. Guo, P.-S. Wang, C.-H. Zhou, Y. Xia, W. Huang, Z. Li, *Sens. Actuators B* **2014**, *203*, 388–395.
[12] M. Y. Elahi, A. Khodadadi, Y. Mortazavi, *J. Electrochem. Soc.* **2014**, *161*, B81–B87.
[13] X. Zhang, Q. Liao, S. Liu, W. Xu, Y. Liu, Y. Zhang, *Anal. Chim. Acta* **2015**, *858*, 49–54.
[14] X. Zhang, R. Ji, L. Wang, L. Yu, J. Wang, B. Geng, G. Wang, *CrystEngComm* **2013**, *15*, 1173–1178.
[15] L. Wang, Y. Zheng, X. Lu, Z. Li, L. Sun, Y. Song, *Sens. Actuators B* **2014**, *195*, 1–7.
[16] F. Sun, L. Li, P. Liu, Y. Lian, *Electroanalysis* **2011**, *23*, 395–401.
[17] C.-L. Sun, W.-L. Cheng, T.-K. Hsu, C.-W. Chang, J.-L. Chang, J.-M. Zen, *Electrochem. Commun.* **2013**, *30*, 91–94.
[18] N. Q. Dung, D. Patil, H. Jung, D. Kim, *Biosens. Bioelectron.* **2013**, *42*, 280–286.
[19] Y.-W. Hsu, T.-K. Hsu, C.-L. Sun, Y.-T. Nien, N.-W. Pu, M.-D. Ger, *Electrochim. Acta* **2012**, *82*, 152–157.
[20] X. Zhou, H. Nie, Z. Yao, Y. Dong, Z. Yang, S. Huang, *Sens. Actuators B* **2012**, *168*, 1–7.
[21] Y. Tian, Y. Liu, W.-P. Wang, X. Zhang, W. Peng, *Electrochim. Acta* **2015**, *156*, 244–251.
[22] Y. Zhao, X. Bo, L. Guo, *Electrochim. Acta* **2015**, *176*, 1272–1279.
[23] Q. Wang, Q. Wang, M. Li, S. Szunerits, R. Boukherroub, *RSC Adv.* **2015**, *5*, 15861–15869.
[24] D. Jiang, Q. Liu, K. Wang, J. Qian, X. Dong, Z. Yang, X. Du, B. Qiu, *Biosens. Bioelectron.* **2014**, *54*, 273–278.
[25] L.-M. Lu, X.-B. Zhang, G.-L. Shen, R.-Q. Yu, *Anal. Chim. Acta* **2012**, *715*, 99–104.
[26] L. Xu, J. Xia, H. Li, H. Li, K. Wang, S. Yin, *Eur. J. Inorg. Chem.* **2011**, *9*, 1361–1365.
[27] J. Luo, S. Jiang, H. Zhang, J. Jiang, X. Liu, *Anal. Chim. Acta* **2012**, *709*, 47–53.
[28] Y. Zhang, L. Su, D. Manuzzi, H. V. E. de los Monteros, W. Jia, D. Huo, C. Hou, Y. Lei, *Biosens. Bioelectron.* **2012**, *31*, 426–432.
[29] J. Bao, C. Hou, Y. Zhang, Q. Li, D. Huo, M. Yang, X. Luo, *J. Electrochem. Soc.* **2015**, *162*, B47–B51.
[30] J. Huang, Z. Dong, Y. Li, J. Li, J. Wang, H. Yang, S. Li, S. Guo, J. Jin, R. Li, *Sens. Actuators B* **2013**, *182*, 618–624.
[31] Z. Fan, B. Liu, X. Liu, Z. Li, H. Wang, S. Yang, J. Wang, *Electrochim. Acta* **2013**, *109*, 602–608.
[32] M. Mohl, P. Pusztai, A. Kukovecz, Z. Konya, J. Kukkola, K. Kordas, R. Vajtai, P. M. Ajayan, *Langmuir* **2010**, *26*, 16496–16502.
[33] A. P. Periasamy, J. Liu, H.-M. Lin, H.-T. Chang, *J. Mater. Chem. A* **2013**, *1*, 5973–5981.
[34] Y. Liu, X. Dong, P. Chen, *Chem. Soc. Rev.* **2012**, *41*, 2283–2307.
[35] C. Chen, Q.-H. Yang, Y. Yang, W. Lv, Y. Wen, P.-X. Hou, M. Wang, H.-M. Cheng, *Adv. Mater.* **2009**, *21*, 3007–3011.
[36] A. R. Rathmell, S. M. Bergin, Y. L. Hua, Z. Y. Li, B. J. Wiley, *Adv. Mater.* **2010**, *22*, 3558–3563.
[37] Y. Xu, K. Sheng, C. Li, G. Shi, *ACS nano* **2010**, *4*, 4324–4330.
[38] H. Gao, Y. Wang, F. Xiao, C. B. Ching, H. Duan, *J. Phys. Chem. C* **2012**, *116*, 7719–7725.
[39] J. Song, L. Xu, C. Zhou, R. Xing, Q. Dai, D. Liu, H. Song, *ACS Appl. Mater. Interfaces*, **2013**, *5*, 12928–12934.
[40] L. Luo, L. Zhu, Z. Wang, *Bioelectrochemistry* **2012**, *88*, 156–163.
[41] H.-X. Wu, W.-M. Cao, Y. Li, G. Liu, Y. Wen, H.-F. Yang, S.-P. Yang, *Electrochim. Acta* **2010**, *55*, 3734–3740.
[42] C. B. Liu, H. Zhang, Y. H. Tang, S. L. Luo, *J. Mater. Chem. A* **2014**, *2*, 4580–4587.
[43] A. J. Bard, L. R. Faulkner, Electrochemical Methods: Fundamentals and Applications, John Wiley, New York, **2001**.
[44] C. H. Xu, B. H. Xu, Y. Gu, Z. G. Xiong, J. Sun, X. S. Zhao, *Energy Environ. Sci.* **2013**, *6*, 1388–1414.
[45] J. Yang, W.-D. Zhang, S. Gunasekaran, *Biosens. Bioelectron.* **2010**, *26*, 279–284.
[46] Y. Zhao, Z. He, Z. Yan, *Analyst* **2013**, *138*, 559–568.
[47] X. Kang, Z. Mai, X. Zou, P. Cai, J. Mo, *Anal. Biochem.* **2007**, *363*, 143–150.
[48] M. Liu, R. Liu, W. Chen, *Biosens. Bioelectron.* **2013**, *45*, 206–212.

Received: February 18, 2016
Accepted: May 2, 2016
Published online: June 7, 2016

